Exploring Radiation-Induced Vulnerabilities in RFICs Through Traditional RF Metrics

Antonio Scialdone, Rudy Ferraro, Luigi Dilillo, Frederic Saigne, Jérôme Boch, Alessandro Masi, and Salvatore Danzeca

***Abstract*— This article describes how to analyze radiation-induced effects using traditional radio-frequency (RF) metrics in RF integrated circuits (RFICs) to be used in the implementation of software-defined radios (SDRs). The impacts of total ionizing dose (TID) and single-event effects (SEEs) on the device characteristics are shown and their consequences for an SDR are discussed. The analysis is based on the error vector magnitude (EVM), carrier frequency offset (CFO), and SEE in the device configuration. It has been applied to the AD9361 RF Agile transceiver. Experimental results are obtained using the high-energy proton beam of 200 MeV at the Paul Scherrer Institute. Two different applications are analyzed to emphasize the impact that radiation effects can have on different communication schemes: quadrature phase shift keying (QPSK) and quadrature amplitude modulation (64-QAM). Results show that single-event transients (SETs) on the analog circuitry of the RF transceiver or single-event upsets (SEUs) inside the configuration registers can lead to EVM degradation. In addition, TID effects lead to frequency drift of the RF carrier, generating an offset between the transmitter and receiver nodes that needs to be taken into account when selecting the recovery algorithms in the receiver.**

***Index Terms*— Error vector magnitude (EVM), frequency offset, radio-frequency integrated circuit (RFIC), single-event effects (SEE), software-defined radio (SDR), total ionizing dose (TID).**

I. Introduction

THE increasing number of connected devices combined with the evolution of multiple radio standards are driving the development of software-defined radios (SDRs) [1]. An SDR is a reconfigurable radio platform where most of the physical layer (PHY) functionalities are implemented with digital signal-processing (DSP) algorithms in programmable electronics like microprocessors or field-programmable gate arrays (FPGAs). This makes possible the implementation of configurable radios where parameters such as operating frequency, modulation scheme, and communication protocol can be changed without any hardware modification. Thus, they represent a good solution for the continuously evolving scenario, where many devices operate over a wide range of frequencies and protocols. With the recent developments of radio-frequency integrated circuits (RFICs), many aspects of the RF front end have become configurable, paving the way for SDRs. However, while their adoption is straightforward in common terrestrial environments, it is not so in space or in particle accelerators where the electronics is subject to radiation-induced effects, such as single-event effects (SEEs) and total ionizing dose (TID) that could make the communication link unreliable. Despite that, these environments would benefit from their application when considering that wired hardware installation, maintenance, and upgrade are not always trivial. Therefore, qualification tests are essential to study the reliability and performance of such devices before using them in a radiation environment. Among the subsystems of an SDR, this work focuses on the RFIC, whose performances have a direct impact on the transmitted/received signal which, in turn, influences the later stage of signal processing in an SDR.

In previous work, Budroweit and Koelpin [2] presented the design challenges of a generic SDR (GSDR) for radiation environments based on the AD9361, a highly integrated RF Agile Transceiver. The transmitter/receiver performances were evaluated at different doses by transmitting/receiving a tone signal at a frequency of 2.4 GHz. For the receiver, the amplitude of the received signal for different gain settings was evaluated. For the transmitter, the intermodulation distortion and output power were measured. Budroweit and Sznajder [3] reported the degradation of these metrics for three different frequencies: 800 MHz, 2.4 GHz, and 5.5 GHz. The GSDR has also been tested in a Mixed-Field Irradiation Environment, emphasizing the impact of radiation effects at the system level [4], showing failures of commercial off-the-shelf (COTS) components or SEEs inducing reset or reconfiguration in the platform. The AD9361 offers a wide range of functionalities that can be accessed through a series of registers. The different failure modes induced by single-event upsets (SEUs) in these registers are analyzed in [5] and [6] under protons and heavy ions, respectively. In addition, in the latter article, the authors use a sine-wave tone to capture the corruption of RF data caused by single-event transients (SETs) on the integrated analog-to-digital converter/digital-to-analog converter (ADC/DAC). A different test was performed instead for the AD9364. The device was used to send an image while being irradiated with heavy ions, and another device was used as a receiver. The test showed that radiation effects could induce corruption in the transmitted signals which would result in a corrupted frame in the received image [7].

Manuscript received 14 February 2023; revised 21 March 2023; accepted 20 April 2023. Date of publication 25 April 2023; date of current version 16 August 2023.

Antonio Scialdone is with the European Organization for Nuclear Research (CERN), CH-1211 Meyrin, Switzerland, and also with the LIRMM, CNRS, and Universite de Montpellier, 34095 Montpellier, France (e-mail: antonio.scialdone@cern.ch).

Rudy Ferraro, Alessandro Masi, and Salvatore Danzeca are with the European Organization for Nuclear Research (CERN), CH-1211 Meyrin, Switzerland.

Luigi Dilillo is with the LIRMM, CNRS, and Universite de Montpellier, 34095 Montpellier, France.

Frederic Saigne and Jérôme Boch are with the CNRS, and Universite de Montpellier, 34095 Montpellier, France.

Color versions of one or more figures in this article are available at https://doi.org/10.1109/TNS.2023.3270206.

Digital Object Identifier 10.1109/TNS.2023.3270206

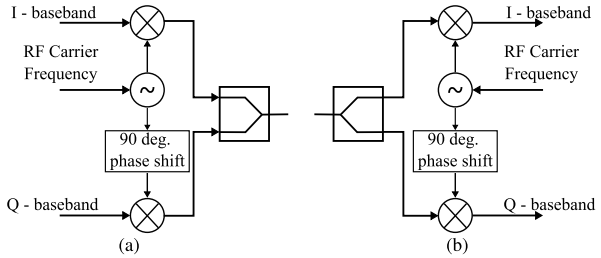

Fig. 1. I–Q modulator and demodulator used in practical transmitter/receiver systems. (a) Modulator. (b) Demodulator.

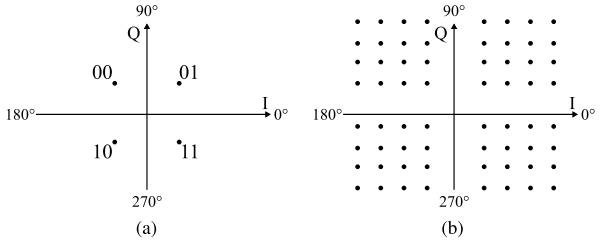

Fig. 2. Constellation diagram of two digital modulation schemes. (a) QPSK with $M = 4$ and (b) 64-QAM with $M = 64$.

However, these tests are not exhaustive for such devices. Depending on their complexity, RFICs may offer multiple features through analog and digital circuits, such as low-noise amplifiers (LNAs), analog/digital filters, and voltage-controlled oscillators (VCOs), whose characteristics are fundamental for the quality of the transmitted/received signal. Nonetheless, the aforementioned tests are not suitable to study their degradation due to radiation effects and the impact of their combined degradation on the communication link. A metric of interest for RF systems is the error vector magnitude (EVM), a system-level metric that gives an overview of the combination of all the system impairments. It measures the device modulation accuracy, and therefore its analysis gives more information on the actual behavior of the device when used for a wireless link, which would be difficult to extrapolate if considering only the degradation of individual components. Practical wireless systems rely on digital modulation, and therefore modulation accuracy is of paramount importance. The validity of the EVM for the radiation effects analysis has already been verified through simulation and experiments in previous works. In [8], the SETs on a silicon-germanium (SiGe) bipolar CMOS (BiCMOS) receiver are evaluated through the analysis of the EVM. In [9] and [10], radiation hardening techniques for the LNAs and VCOs, respectively, are proposed based on the EVM evaluation. However, these works are focused on the receiver side and are not considering the impact of the transmitter degradation in an SDR application.

The objective of this work is to demonstrate how traditional RF metrics can be used to explore the radiation-induced vulnerabilities in RFICs, illustrating how the radiation effects can impact the device characteristics and how these should be analyzed before using the device for a real application.

II. Digital Communication Background

RF communication systems share the common goal of placing digital information onto an RF carrier and recovering it with accuracy. There are three main steps to convey information over the air.

1) A carrier is generated at the transmitter.
2) *Modulation:* Data are modulated on the carrier by changing its characteristics, that is, frequency/phase and/or amplitude.
3) *Demodulation:* Data are demodulated by detecting such changes at the receiver.

In digital communications, both phase and amplitude changes are used. In practical systems, this is accomplished using an in-phase (I) and quadrature (Q) modulator, shown in Fig. 1(a). A local oscillator (LO) is used to generate the carrier signal at RF, and a 90° phase shifter is placed on one of the two paths. Two baseband signals, I and Q, are upconverted and mixed. Two signals separated by 90° are independent of each other, thus they can be combined into a single output, and they will not interfere with each other. With such an architecture, digital modulation is easily accomplished. Binary data are mapped into a set of M discrete points (symbols) on the I/Q plane, also known as a constellation diagram. Moving between points causes a change in amplitude, phase, or both.

There are multiple types of digital modulation schemes used nowadays in wireless communications [11]. Two examples are quadrature phase shift keying (QPSK) commonly used in satellite communications and quadrature amplitude modulation (QAM) used in high-data-rate systems. Their constellation diagrams are shown in Fig. 2(a) and (b), respectively. At the receiver, the composite signal is mixed with the local oscillator, and it goes through an IQ demodulator shown in Fig. 1(b), that separates the I and Q components. These are sampled and transferred to the digital domain. Digital bits will then be recovered based on the received symbols' location on the constellation diagram. Therefore, one must accurately determine the magnitude and phase of the received signal to demodulate data correctly.

III. Radiation Effects and Test Methodology

In an RF circuit, there are multiple sources of errors to take into account when operating in a radiation environment. This section describes the radiation effects on the RF circuitry and how they can be identified. Moreover, their impact on digital communication is explained to emphasize what are the consequences when the device is used for an SDR platform.

A. Radiation Effects on an RF Transceiver

Even though impairments are addressed during the design stage of the RF transceiver [12], radiation effects can change the characteristics of the device. The degradation in terms of frequency, amplitude, and phase noise of a VCO with TID is reported in [13]. The VCO is fundamental in phase-locked loops (PLL) systems because it must provide a stable LO for up/downconversion of the signal, and noise on the VCO can corrupt the transmitted/received signal. VCOs are also sensitive to SETs as reported in [14]. In [15], the authors report the TID degradation of various PLL integrated circuits (ICs), while results for a SEE-hardened PLL are reported in [16]. Another block for an RF receiver is the LNA, whose role is to increase the gain while minimizing the added noise for the following stages. However, there can be degradation of gain and noise features with exposition to TID, as shown in [17].

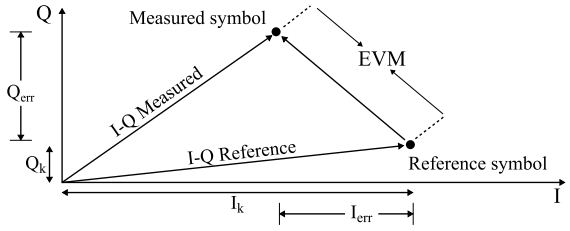

Fig. 3. Graphical representation of the EVM. The reference symbol is the location of the symbol in the ideal condition.

In addition, ADC/DAC can be affected by SETs as discussed in [18], leading to wrong IQ samples when used in an IQ modulator/demodulator as reported in [6] for the AD9361. All these impairments are reflected in a change in amplitude/phase of the transmitted/received signal, thus they are visible on the constellation diagram. One metric that can be used for their evaluation is the EVM. It gives an insight into the combined impact of all the impairments, that is, LO phase noise and amplifier compression, on the system performance, therefore it is used to identify and correct such issues at the design stage [19]. The EVM measures the deviation of the received symbol from its ideal location. Fig. 3 shows its graphical representation. It is measured as

$$\mathrm{EVM}_{\mathrm{rms}}(\%) = \sqrt{\frac{\frac{1}{N}\sum_{k=1}^{N} I_{\mathrm{err}}^2 + Q_{\mathrm{err}}^2}{\frac{1}{N}\sum_{k=1}^{N}\left(I_k^2 + Q_k^2\right)}} \times 100$$

where N is the number of symbols taken into account for the measurement. The acceptable range of EVM depends on the modulation order and the specific application. A communication system based on QPSK may tolerate a higher EVM compared to an application based on 64-QAM because the decision boundaries for a 64-QAM modulation give less margin for errors. On the other hand, for a QPSK modulation, a symbol is correctly decoded if it falls in the correct part of the diagram, no matter how far from the reference symbol. Thus, there are different requirements for the EVM, as defined by the European Telecommunications Standards Institute (ETSI) standards [20]. The higher the modulation order, the stricter the requirements on the EVM.

Recent RFICs allow the configuration of parameters such as carrier frequency, sampling rate, gain settings, and digital/analog filtering bandwidth. These parameters are controlled through a set of configuration registers that if affected by an SEU may lead to a failure. Depending on the register functionality, different recovery mechanisms may be necessary. Those related to the device configuration, such as carrier frequency or sampling rate, are essentials for the communication link and, whether affected by an SEU, they need to be reconfigured to reestablish the connection. Those registers, which contain status information instead, do not cause any visible failure. Finally, some other registers' upsets may induce changes that are not recoverable through reconfiguration and require a reinitialization/recalibration of the device. In this work, this event is referred to as a single-event functional interrupt (SEFI). Such typologies have already been identified in [5] for the AD9361. In addition, SEUs inside the IC can cause single-event latchups (SELs), leading to device failure.

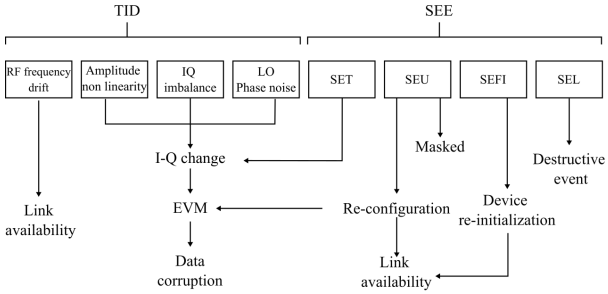

Fig. 4. Source of errors in an RFIC and impairments caused by TID and SEE. Each error can have different consequences on the communication link.

B. Radiation Effects Impact on Digital Communication

In practical communication systems, the transmitter and the receiver are implemented on two different nodes. Consequently, they use clock signals that are not exactly matched in phase and frequency, requiring different recovery stages before data demodulation [21]. The receiver should sample the incoming signal at the correct instant in time to successfully recover the data. A wrong sampling time on the receiver results in clustering or scattering of the symbols in the constellation diagram. Therefore, algorithms exist to perform symbol recovery based on the received signal such as the Mueller and Muller [22] or the Gardner [23]. In addition to symbol recovery, although set at the same frequency, the LOs of the two devices cannot oscillate at the very same frequency. On the contrary, for a set RF carrier frequency f_c, the two nodes exhibit a relative frequency offset known as carrier frequency offset (CFO). Such offset should be compensated before data demodulation, and different carrier recovery algorithm exists such as scanning techniques or PLL-based loops [24]. After the recovery stages, data can be demodulated. However, these algorithms have different performances depending on the entity of the error. This is true, especially for PLL-based loops that need some time to produce a stable solution. Therefore, their usage should be tailored to the specific application. Nonetheless, the situation is complicated when the device is exposed to radiation. SEEs on the RF transceiver may cause glitches on the IQ symbols disrupting the downstream algorithms which are not supposed to deal with abrupt changes. TID effects instead can degrade the device characteristics, leading to a higher convergence time or the loss of the communication link in case the algorithm is not capable of correcting a large error.

All these aspects should be taken into consideration when using an RFIC in a radiation environment because they may affect the performance of the communication link. Fig. 4 summarizes what are the different impairments and their consequences. The remainder of this article focuses on the analysis of EVM, RF frequency drift, SET, and SEU from the perspective of implementing an SDR application.

IV. DUT and Test Setup

The device under test (DUT) is the AD9361 Agile Transceiver from Analog Devices. It combines an RF front-end with a mixed-signal baseband section providing a low-voltage differential signaling (LVDS)/complementary metal–oxide–semiconductor (CMOS) interface for a processor/FPGA. It includes two independent receiver (RX) and transmitter (TX)

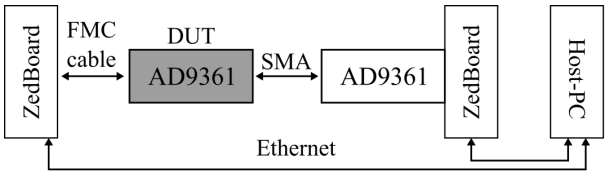

Fig. 5. Overview of the setup used during the radiation test campaign.

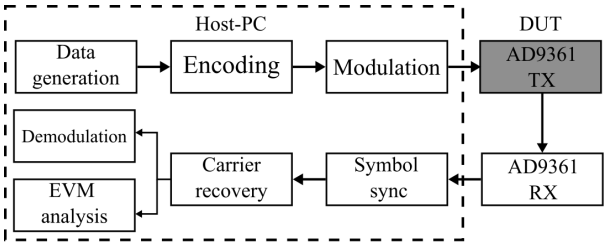

Fig. 6. Data flow used during the test. Data are generated on the host PC, transmitted to the DUT and received by the RX (not irradiated). In postprocessing, data go through recovery stages and the EVM is analyzed.

chains. Two separate LOs with an operating range between 70 MHz and 6 GHz are used for the TX and RX paths, making it suitable for a wide range of applications. A single LO is used to define the sampling rate of the ADC and DAC. The device embeds a chain of digital filters necessary to match the sample rate of the ADC/DAC with the speed of the digital interface, and an additional filter that can be configured by the user for custom applications. The device features an automatic gain control (AGC) mechanism to handle a wide range of signal levels on the RX path. It acts by adjusting the gain of the different stages based on the received signal to avoid high signal distortion. The RX chains include circuitry for dc and quadrature correction. The device parameters, that is, sampling rate, RF carrier frequency, gain, and attenuation, can be configured via a set of registers accessible through a serial peripheral interface (SPI). However, given the complexity and the high number of registers of the device, high-level application programming interface (APIs) are provided by the manufacturer to set parameters such as frequency, gain, and bandwidth, hiding the low-level implementation from the user.

The AD-FMCOMMS3-EBZ board has been used to perform the radiation test campaign. It is an evaluation kit for the AD9361 designed as an FPGA mezzanine card (FMC). The DUT is connected to the ZedBoard, a development kit based on the Xilinx Zynq-7000 system-on-chip (SoC), which contains an ARM Cortex-A9 CPU coupled with an FPGA. The FPGA implements the interface and SPI communication with the DUT, whereas the processor is used to transfer data between the FPGA and the host PC through Ethernet. The test setup consists of two AD9361 acting as TX and RX, respectively. The devices are interconnected using SMA-to-SMA cables. Only one device was placed under radiation, and its configuration was changed depending on the test. A schematic of the test setup is shown in Fig. 5. Since the device can be used for a wide range of applications, two different applications employing different data-processing algorithms have been tested to evaluate the impact of radiation effects on different communication systems.

The first application is based on QPSK modulation, commonly used in time-division multiple access (TDMA) systems like satellites. The second application is based on the long-term evolution (LTE) protocol, that is, a standard for wireless communication for mobile devices. It is based on the principle of orthogonal-frequency-division multiplexing (OFDM) [25]. In this kind of communication system, multiple orthogonal carriers are transmitted to send data in parallel. These carriers are separated from each other by a guard frequency so that they do not interfere with each other. The standard specifications are defined in the TS36.104 document [20]. It describes in detail the test waveforms to be used to assess whether a device can be used or not within the LTE network. For each test model, the EVM requirements are reported. In this work, the test model 3.1 has been used, which is based on a 64-QAM modulation and with a subcarrier spacing of 15 kHz.

For all the irradiation runs, the baseband algorithms necessary for data modulation/demodulation are performed entirely on the host PC using MATLAB, whereas the FPGA is used to exchange data with AD9361. A random payload is generated, encoded, and modulated according to the application being implemented. The data are then stored inside the FPGA, and the TX is configured in cyclic mode, that is, sending the same buffer repeatedly. The irradiation is stopped either manually because of a radiation-induced error that interrupts the transmission or because the target fluence has been reached. The RX instead is configured to continuously receive and save data, without performing data processing during irradiation. This choice was taken to increase the receiver acquisition rate which would be much lower if data processing was performed in between receptions. The entire data flow is shown in Fig. 6. For both applications, the RF carrier frequency was set to 2.4 GHz, and a variable number of packets was transmitted/received, depending on the length of the irradiation.

The data-processing algorithms are different between the two applications. In the case of QPSK, the symbol recovery block implements a PLL-based algorithm to correct the symbol error using the Gardner technique. The carrier recovery instead is split into a coarse and fine frequency correction. The first detects and corrects the frequency offset using an FFT-based method. This is usually necessary if the offset between the two nodes is large. The smaller offset is removed by the fine frequency correction that uses a PLL-based loop to produce a stable constellation diagram. The two parameters to fix for the PLL-based algorithms are the damping factor ζ and the loop bandwidth B_{Loop}. As described in [24], these two parameters define the convergence and reaction time of the algorithm, and they should be tailored to the specific application. In this work, an EVM below 5% was obtained preirradiation using $\zeta = 0.7$ and $B_{\text{Loop}} = 0.01$, which are the values used for the analysis.

Concerning the LTE application, the MATLAB LTE Toolbox has been used for both data generation and analysis. It can generate and analyze the waveforms defined by the LTE standard, determining the EVM and providing an estimate of the sampling and frequency offset. In particular, the frequency offset is corrected using the Cyclic Prefix technique described in [26], whereas the sampling error is determined using an FFT-based method. For the LTE application only, a test aiming at calculating the frequency offset between the

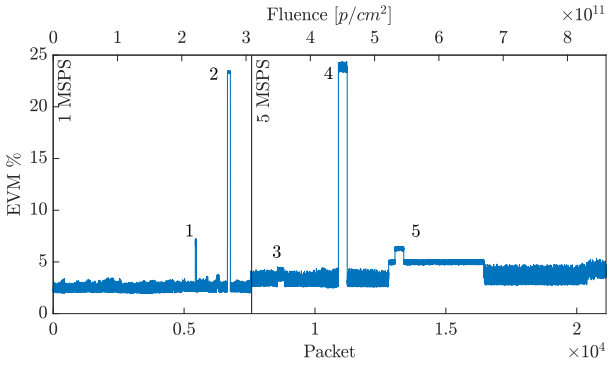

Fig. 7. EVM for all the packets received during the experiment using QPSK modulation at two different sampling rates. Abrupt changes (numbered from 1 to 5) correspond to SEUs in the device configuration. A slight increase can be observed toward the end, at 500 Gy, due to performance degradation with the cumulated dose.

two nodes has been performed. The test consists in transmitting/receiving the LTE waveform changing the RF carrier frequency from 100 MHz to 6 GHz, in steps of 100 MHz.

For both applications, a background script has been used to read all the configuration registers during irradiation. In this way, it is possible to correlate whether SEUs in the configuration registers could affect the communication link. Moreover, the device was reconfigured through the high-level APIs to recover the functionalities in case they were lost because of radiation-induced errors. The configuration was triggered every 200 packets in the case of QPSK, and at every packet in the case of the QAM.

V. Test Results

Two different DUTs have been tested to analyze the QPSK and QAM application, respectively. The devices have been tested at the Paul Scherrer Institute (PSI) in Villigen, Switzerland, under a high-energy proton beam of 200 MeV.

A. QPSK-Based Application

Concerning the QPSK application, the DUT has been tested at two different sampling rates of 1 and 5 MSPS, respectively, accumulating a total dose of 500 Gy. Fig. 7 reports the root mean square (rms) EVM of all the packets received as a function of the fluence and for the two sampling rates. The EVM is computed over all the symbols within a packet (12 800 bits corresponding to 6400 symbols) and expressed in percentage. At the start of irradiation, the measured EVM is below 5% as was the case before irradiation. A shift of EVM can be observed in correspondence to the change in the sampling rate. Therefore, the increase in EVM can be related to a different sampling rate rather than to TID degradation. At the end of irradiation, at 500 Gy, a slight increase in EVM has been measured with the same configuration. This may be the indication of some degradation in the transmitter due to the accumulated dose, leading to worse performance.

In addition, some abrupt changes, marked with numbers in the figure, can be observed. These can be related to SEUs inside the configuration registers of the RFIC.

Fig. 8 shows the EVM of the packets received during one of the events. As it can be seen, once the reconfiguration is triggered, the EVM is restored to normal values, confirming

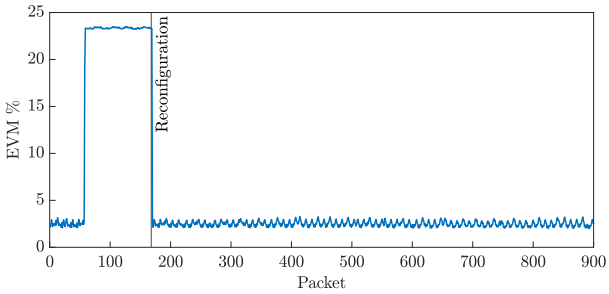

Fig. 8. EVM before and after the device reconfiguration corresponding to event number 2. The EVM is restored once the device is reconfigured, indicating that the performance degradation is due to an SEU in the device configuration.

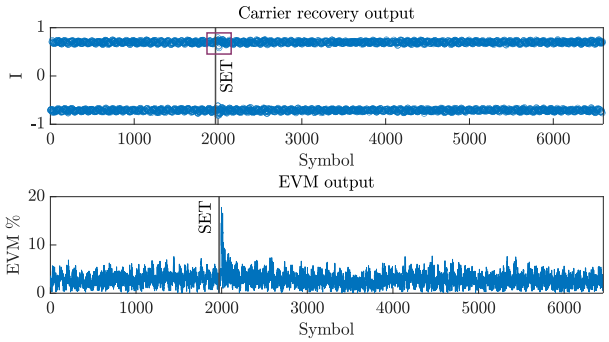

Fig. 9. Analysis of an SET on the analog circuitry through the EVM of individual symbols within a packet (6400 symbols). On top, the output of the carrier recovery algorithm, showing the effect of an SET that disrupts the feedback loop. This causes an increase of EVM (bottom) for some symbols of the packet until the algorithm converges again.

that the change was due to an SEU in the device configuration. Nonetheless, the payload could still be recovered correctly. The DUT register analysis showed that an SEU likely occurred in the gain control registers, which was corrected through reconfiguration. On the other hand, event 5 lasted longer, despite the reconfiguration. Analyzing the register values in correspondence of such an event, it was not possible to identify the register causing the issue because many of them changed values. However, since the device behavior was restored later, it is likely that additional changes were performed by the low-level drivers when the next reconfiguration was triggered.

Besides the packet EVM, monitoring the EVM of individual symbols within a packet can help detect SET on the transmitter and its impact on the receiver. Fig. 9 shows an SET captured in this way. The received data go through a series of DSP algorithms, which are disturbed by abrupt changes in the incoming signal. The output of the carrier recovery algorithm (top) is a stable constellation until the SET causes the output to oscillate. Thus, the corresponding symbol has a higher EVM (bottom) compared to the other symbols within the received packet. However, when the algorithm converges again, the EVM returns below 5%. Despite the event, the affected packet could still be retrieved correctly. Table I reports the cross section for the two categories of events, SETs and SEUs, observed during the test with the corresponding 95% confidence interval [27].

B. QAM-Based Application

A second DUT has been used to investigate the EVM of the QAM application and to retrieve the CFO. For this purpose,

TABLE I

CROSS SECTIONS FOR THE TWO CATEGORIES OF THE SEE OBSERVED WITH A PROTON FLUX OF 3.86×10^8 p/cm^2/s DURING THE QPSK TEST

Type	Fluence $[p/cm^2]$	# Events	σ $(cm^2/device)$		
			Lower limit	σ	Upper limit
SET	$8.60 \cdot 10^{11}$	1	$2.34 \cdot 10^{-14}$	$1.16 \cdot 10^{-12}$	$6.47 \cdot 10^{-12}$
SEU		5	$1.85 \cdot 10^{-12}$	$5.81 \cdot 10^{-12}$	$1.36 \cdot 10^{-11}$

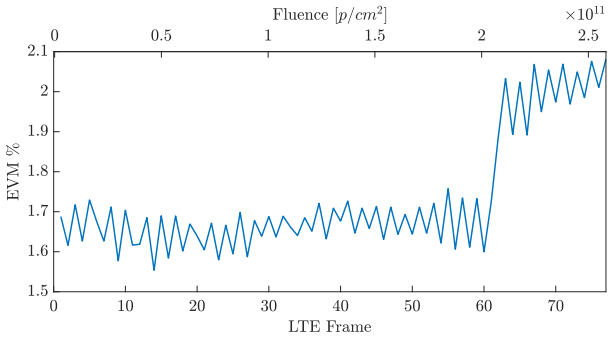

Fig. 10. EVM evolution for the LTE frames received during irradiation for a fluence of $2.58 \cdot 10^{11}$ p/cm^2. A slight increase in EVM is measured toward the end, at 500 Gy, due to transmitter degradation.

the irradiation was stopped at 70–150–300 and 520 Gy, respectively, to measure the TX LO offset over the device frequency range. In between the steps, this DUT was initially configured for a QPSK application in the receiver mode, whose results are not presented because they are not in the scope of this article. After 400 Gy, the DUT was configured for QAM to evaluate the EVM response against the SEE.

Concerning the TID effects on EVM, it was retrieved at different dose steps, and the device did not exhibit large variations between 0 and 520 Gy, where the EVM was measured as 1.6% and 2.1%, respectively.

Concerning the SEE response, the device was exposed to a fluence of $2.58 \cdot 10^{11}$ p/cm^2 and the EVM response is presented in Fig. 10. The fluence reached was lower compared to the QPSK application because of a facility issue.

As visible in the figure, no significant change as in the QPSK case was observed. However, at around 500 Gy, a small variation of EVM was measured, which is likely due to TID degradation since neither reconfiguration nor power cycle restored the previous condition. Moreover, it occurred around the same cumulated TID level for the DUT used in the QPSK test. The lack of events could be due to the lower fluence reached.

Concerning the frequency offset, Fig. 11 reports the CFO measured at different dose steps expressed as part per million (PPM), which can be used to relate the CFO to the carrier frequency f_c as

$$\text{CFO} = \frac{\text{PPM} \times f_c}{10^6}.$$

As can be seen, the offset increases with the accumulated dose, indicating degradation of the TX LO. Moreover, the variation is higher at higher RF frequencies.

C. SEE on Device Configuration

A separate analysis has been conducted on the SEE on the configuration registers. The events are collected by reading

TABLE II

CROSS SECTION FOR THE TWO CATEGORIES OF EVENTS OBSERVED WITH A PROTON FLUX OF $3.86 \cdot 10^8$ p/cm^2/s ON THE TWO DUTS

Type	Fluence $[p/cm^2]$	# Events	σ $(cm^2/device)$		
			Lower limit	σ	Upper limit
Reconfiguration - QPSK	$8.60 \cdot 10^{11}$	5	$1.85 \cdot 10^{-12}$	$5.81 \cdot 10^{-12}$	$1.36 \cdot 10^{-11}$
Reconfiguration - QAM	$2.58 \cdot 10^{11}$	0	-	-	$1.43 \cdot 10^{-11}$
Re-initialization	$1.12 \cdot 10^{12}$	13	$6.06 \cdot 10^{-12}$	$1.16 \cdot 10^{-11}$	$1.99 \cdot 10^{-11}$
Permanent failure		3	$5.35 \cdot 10^{-13}$	$2.68 \cdot 10^{-12}$	$7.83 \cdot 10^{-12}$

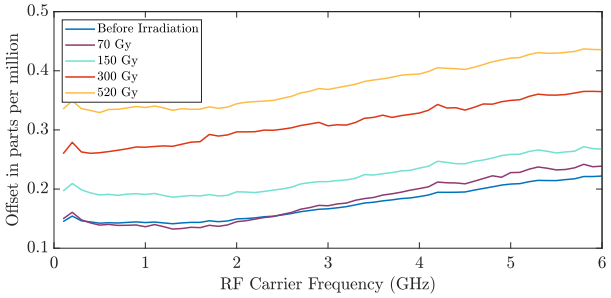

Fig. 11. CFO estimation based on the Cyclic Prefix algorithm for different doses over the entire device frequency range (100 MHz–6 GHz). The offset varies with the dose, and it increases with the RF carrier frequency.

all the registers through the SPI and comparing their value with their initial configuration. The device contains status and configuration registers. The bits in the status register change continuously, and they do not correspond to parameters that can affect the device functioning, and therefore they have not been considered for the SEE analysis. Conversely, SEEs on configuration registers may have an important impact, which can be grouped into three categories, depending on their effect on the communication link. This differentiation comes from the analysis of the different events that have been observed during the irradiation. Their cross section is reported in Table II with the 95% confidence interval. The first category causes a change in the device configuration, which does not lead to a failure in the transmission, but rather to performance degradation. Moreover, these may have different impacts depending on the modulation. An example is the change of gain configuration of the device that occurred during the QPSK test. No event was observed during the QAM test, probably because of the lower fluence reached as previously mentioned. The second and third categories instead are independent of the modulation. The second category induces the complete loss of transmission. One example is the register handling the configuration for the LVDS interface that was affected by an SEU causing the inversion of the LVDS lines. The third category of the SEE causes the device to be no longer recognized by the host PC. Each category has a different recovery mechanism. In the first case, the configuration change can be detected by monitoring changes in the EVM, and reconfiguration of the register is sufficient to restore the working conditions. For the second category, the device must be reinitialized, which can be done through the dedicated pin available on the IC. Finally, the third type causes a failure in the device that cannot be recognized anymore by the controlling FPGA, and no reconfiguration is possible. Thus, in this case, a power cycle is necessary.

VI. DISCUSSION

Experimental results show that the EVM did not exhibit large variation up to 500 Gy. A slight variation of EVM has

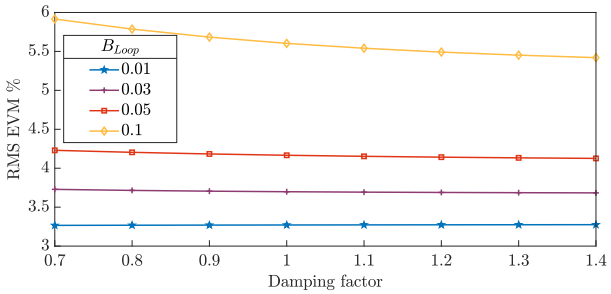

Fig. 12. EVM of the packet affected by an SET computed for different values of loop bandwidth and damping factor of the recovery algorithm. For lower values of B_{Loop}, the receiver reacts faster to the transient, producing a lower EVM.

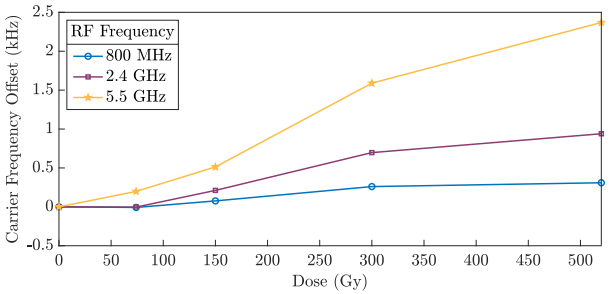

Fig. 13. CFO estimation based on the Cyclic Prefix correlation for three carrier frequencies at different doses. For higher frequencies, the frequency offset is larger at higher doses.

been measured around 500 Gy for both applications, which can be related to performance degradation. In both cases, all the packets have been recovered without any error inside the payload.

During the QPSK test, an increase in EVM due to the SEU in the device configuration has been observed. This can be explained by the fact that the RFIC has many configuration registers that, if affected by an SEU, modify the transmitted signal. As an example, one SEU increased the transmitter gain leading to the saturation of the receiver and a worse received signal. As a consequence, the EVM measured after the recovery algorithm was higher. Even though it was not the case, the data can be corrupted with a higher EVM. As discussed in [28], the EVM of a communication system is related to its bit error rate (BER). Clearly, the higher the EVM, the higher the BER. Thus, one can use the EVM degradation to retrieve the BER estimation for its communication system.

Concerning the observed SETs, the same event has been categorized as an SEFI $I\,Q$ in a previous work [5] where a sine wave was transmitted and received to detect glitches on the $I\,Q$ lines. However, when using modulated data, as is the case in practical systems, it is difficult to interpret SET by analyzing the $I\,Q$ waveforms directly because they oscillate between multiple levels of amplitude and phase. However, using the EVM approach, one can easily detect spikes in the EVM and correlate them with SET. This is helpful to understand how DSP algorithms implemented on the receiver behave when an SET occurs on the transmitter. PLL-based algorithms are based on feedback loops. The main idea is to gradually adjust the incoming signal based on an error estimation computed for each sample. Therefore, the algorithm response will be different depending on the input. Taking as an example the frequency recovery algorithm implemented in this work, the two parameters that can be used to tune the algorithm are the loop bandwidth B_{Loop}, which determines the convergence time, and the damping factor ζ, which determines the reaction time. Fig. 12 reports the packet EVM affected by the SET for different values of B_{Loop} as a function of ζ. It was obtained by processing the received data with the same recovery algorithm but with different parameters. As can be seen, the rms EVM increases by increasing B_{Loop}, because after the SET occurs, the algorithm does not converge to a stable and clean solution. Reducing B_{Loop}, the corrected signal is less noisy, producing a better EVM. With this analysis, one can study the SET response of a particular system and implement the receiver accordingly.

Another consideration should be made for the recovery algorithms necessary for frequency offset corrections. In particular, the analysis refers to the signal after a carrier recovery phase employing both coarse and fine frequency correction. At first, the large offset is estimated and corrected using an FFT-based method, whereas the remaining offset is corrected through a PLL-based algorithm. However, this is not always the case since the choice of the recovery stages depends on the application. Nonetheless, it may happen that the offset becomes larger than what can be compensated. This was the case for the QPSK application, where an SEU in the device configuration caused a sudden shift of the carrier frequency, and the PLL-based algorithm alone was not able to compensate for the offset. In a system without a coarse frequency correction stage, this event would cause a loss of communication until the device is reconfigured. In addition to that, it has been observed that the CFO increases with the cumulated dose. Therefore, one should take into account the expected dose and choose the recovery stages accordingly. Nonetheless, the FFT-based method is resource-intensive and requires more data to estimate the offset compared to a PLL-based algorithm that works on one sample at a time. In a practical system, these algorithms will be implemented either in an FPGA or a microprocessor. Therefore, one should consider the tradeoff between the available resources and the lifetime required for the communication link before choosing the implementation.

The same discussion could be done for the LTE application. Fig. 13 reports the CFO for three carrier frequencies at different doses. To compensate for this offset before data demodulation, the Cyclic Prefix is included in OFDM systems. The cyclic prefix is added by extending each symbol with a prefix, that is, a repetition of the last symbols, and it can be used to estimate and correct the frequency offsets between the two devices. However, such estimation works only if

$$f_{\text{off}} < \frac{\Delta F}{2}$$

where ΔF is the subcarrier spacing, which is 15 kHz for the adopted LTE waveform. In case the offset is bigger, the estimation and the data decoding DSP algorithms will fail. Moreover, if a CFO is present, this impairs the orthogonality of the subcarriers resulting in intercarrier interference, leading to performance degradation as discussed in [29]. Despite that, this was not the case for the DUT. The maximum drift,

25% of the threshold, was observed at 5.5 GHz reached after a cumulative dose of 520 Gy. In case it would have been higher, a possible solution is to use a pilot carrier that can help estimate the larger offset [30], followed by the CP algorithm to recover the remaining frequency offset.

VII. Conclusion

In this work, it has been shown how radiation-induced impairments on RFICs can be studied through traditional RF metrics such as EVM and CFO. Experimental results have been presented and analyzed to show the impact of such impairments on a communication system. Two different applications using the AD9361 have been tested: one based on a QPSK modulation and one based on the LTE protocol. Analyzing the EVM of the device when running the two applications, it is possible to identify SEU, SET, and TID effects on the DUT and study their impact on the communication link. For the QPSK-based model, SETs on the analog circuit have been observed through the EVM analysis. Transient on the IQ lines disrupts the data recovery stages of an SDR, affecting the EVM directly. Abrupt changes on the EVM have been measured in correspondence to SEUs in the device configuration. No large variation of the modulation accuracy has been observed for both applications up to a total dose of 500 Gy, when worse performance has been measured. In addition to the EVM analysis, an increase in the RF frequency drift with the dose has been observed. However, it did not lead to the failure of the link because the drift was lower than the failure threshold for the recovery algorithms employed. Nonetheless, for the QPSK application, an SEU in the device configuration caused the drift to be larger than what could be compensated, requiring an additional recovery stage.

References

[1] T. Ulversøy, "Software defined radio: Challenges and opportunities," *IEEE Commun. Surveys Tuts.*, vol. 12, no. 4, pp. 531–550, 4th Quart., 2010.

[2] J. Budroweit and A. Koelpin, "Design challenges of a highly integrated SDR platform for multiband spacecraft applications in radiation enviroments," in *Proc. IEEE Topical Workshop Internet Space (TWIOS)*, Jan. 2018, pp. 9–12.

[3] J. Budroweit and M. Sznajder, "Total ionizing dose effects on a highly integrated RF transceiver for small satellite radio applications in low Earth orbit," in *Proc. IEEE Int. Symp. Phys. Failure Anal. Integr. Circuits (IPFA)*, Jul. 2018, pp. 1–6.

[4] J. Budroweit, S. Mueller, M. Jaksch, R. G. Alía, A. Coronetti, and A. Koelpin, "In-situ testing of a multi-band software-defined radio platform in a mixed-field irradiation environment," *Aerospace*, vol. 6, no. 10, Sep. 2019, Art. no. 106.

[5] J. Budroweit, M. P. Jaksch, and M. Sznajder, "Proton induced single event effect characterization on a highly integrated RF-transceiver," *Electronics*, vol. 8, no. 5, May 2019, Art. no. 519.

[6] J. Budroweit, M. Jaksch, R. G. Alía, A. Coronetti, and A. Kölpin, "Heavy ion induced single event effects characterization on an RF-agile transceiver for flexible multi-band radio systems in NewSpace avionics," *Aerospace*, vol. 7, no. 2, Feb. 2020, Art. no. 14.

[7] D. Chen, T. Mondy, and A. Phan, "Heavy ion test report for the AD9364 RF transceiver," NASA, Washington, DC, USA, Tech. Rep. GSFC-E-DAA-TN44752, 2017. [Online]. Available: https://ntrs.nasa.gov/api/citations/20170009007/downloads/20170009007.pdf

[8] A. Ildefonso et al., "Modeling single-event transient propagation in a SiGe BiCMOS direct-conversion receiver," *IEEE Trans. Nucl. Sci.*, vol. 64, no. 8, pp. 2079–2088, Aug. 2017.

[9] P. K. C. Mishu et al., "Voltage-controlled oscillator utilizing inverse-mode SiGe-HBT biasing circuit for the mitigation of single-event effects," *IEEE Trans. Nucl. Sci.*, vol. 69, no. 6, pp. 1242–1248, Jun. 2022.

[10] A. Ildefonso et al., "Tradeoffs between RF performance and SET robustness in low-noise amplifiers in a complementary SiGe BiCMOS platform," *IEEE Trans. Nucl. Sci.*, vol. 67, no. 7, pp. 1521–1529, Jul. 2020.

[11] M. Barnela and D. S. Kumar, "Digital modulation schemes employed in wireless communication: A literature review," *Int. J. Wired Wireless Commun.*, vol. 2, no. 2, pp. 15–21, Apr. 2014.

[12] T. H. Lee, *The Design of CMOS Radio-Frequency Integrated Circuits*, 2nd ed. Cambridge, U.K.: Cambridge Univ. Press, 2003.

[13] S. Jagannathan et al., "Sensitivity of high-frequency RF circuits to total ionizing dose degradation," *IEEE Trans. Nucl. Sci.*, vol. 60, no. 6, pp. 4498–4504, Dec. 2013.

[14] W. Chen et al., "Investigation of single-event transients in voltage-controlled oscillators," *IEEE Trans. Nucl. Sci.*, vol. 50, no. 6, pp. 2081–2087, Dec. 2003.

[15] D. I. Sotskov et al., "Total ionizing dose effects in phase-locked loop ICs and frequency synthesizers," in *Proc. 15th Eur. Conf. Radiat. Effects Compon. Syst. (RADECS)*, Sep. 2015, pp. 367–370.

[16] Z. Chen et al., "Study of total-ionizing-dose effects on a single-event-hardened phase-locked loop," *IEEE Trans. Nucl. Sci.*, vol. 65, no. 4, pp. 997–1004, Apr. 2018.

[17] A. S. Youssouf, M. H. Habaebi, and N. F. Hasbullah, "The radiation effect on low noise amplifier implemented in the space-aerial–terrestrial integrated 5G networks," *IEEE Access*, vol. 9, pp. 46641–46651, 2021.

[18] T. L. Turflinger, M. V. Davey, and B. M. Mappes, "Single event effects in analog-to-digital converters: Device performance and system impact," *IEEE Trans. Nucl. Sci.*, vol. 41, no. 6, pp. 2187–2194, Dec. 1994.

[19] "Software defined radio measurement solutions," Keysight Technol., Santa Rosa, CA, USA, Appl. Note 5989-6931, 2017. [Online]. Available: https://www.keysight.com/ch/de/assets/7018-01616/application-notes/5989-6931.pdf

[20] "Evolved universal terrestrial radio access (E-UTRA)," Eur. Telecommun. Standards Inst., Sophia Antipolis, France, Tech. Rep. RTS/TSGR-0436104v830, 2008. [Online]. Available: https://www.etsi.org/deliver/etsi_ts/136100_136199/136104/08.03.00_60/ts_136104v080300p.pdf

[21] J. Proakis and M. Salehi, *Digital Communication*, 5th ed. New York, NY, USA: McGraw-Hill, 2007.

[22] K. Mueller and M. Müller, "Timing recovery in digital synchronous data receivers," *IEEE Trans. Commun.*, vol. COM-24, no. 5, pp. 516–531, May 1976.

[23] F. Gardner, "A BPSK/QPSK timing-error detector for sampled receivers," *IEEE Trans. Commun.*, vol. COM-34, no. 5, pp. 423–429, May 1986.

[24] M. Rice, *Digital Communications: A Discrete-Time Approach*. London, U.K.: Pearson, 2009.

[25] S. B. Weinstein, "The history of orthogonal frequency-division multiplexing [history of communications]," *IEEE Commun. Mag.*, vol. 47, no. 11, pp. 26–35, Nov. 2009.

[26] J. J. van de Beek, M. Sandell, and P. O. Börjesson, "ML estimation of time and frequency offset in OFDM systems," *IEEE Trans. Signal Process.*, vol. 45, no. 7, pp. 1800–1805, Nov. 1997.

[27] "Single event effects test method and guidelines—Basic specification," Eur. Space Agency, Paris, France, Tech. Rep. 25100, 1995. [Online]. Available: https://escies.org/download/webDocumentFile?id=62690

[28] R. A. Shafik, M. S. Rahman, and A. R. Islam, "On the extended relationships among EVM, BER and SNR as performance metrics," in *Proc. Int. Conf. Electr. Comput. Eng.*, Dec. 2006, pp. 408–411.

[29] T. Pollet and M. Moeneclaey, "The effect of carrier frequency offset on the performance of band limited single carrier and OFDM signals," in *Proc. IEEE Global Telecommun. Conf. (GLOBECOM)*, vol. 1, Nov. 1996, pp. 719–723.

[30] C. Li and T.-S. Ng, "Pilot-based carrier frequency offset estimation in OFDM systems," in *Proc. 4th Int. Conf. Inf., Commun. Signal Process., 4th Pacific Rim Conf. Multimedia*, 2003, pp. 874–878.